OBSERVATIONS OF THE ANISOTROPY IN THE COSMIC MICROWAVE BACKGROUND BY THE FIRS, SK93, and MSAM-I EXPERIMENTS

Case Western Reserve University, April 1994

Lyman Page
Department of Physics, Princeton University
Princeton, NJ, 08544

Experimental teams

FIRS: Ed Cheng[a], Ken Ganga[b], Stephan Meyer[c] & Lyman Page[b]

SK93: Norm Jarosik[b], Barth Netterfield[b], Lyman Page[b], Dave Wilkinson[b] & Ed Wollack[b]

MSAM-I: Ed Cheng[a], David Cottingham[d], Dale Fixsen[e], Casey Inman[c], Matt Kowitt[a], Steve Meyer[c], Lyman Page[b], Jason Puchalla[c], & Bob Silverberg[a]

ABSTRACT

The observations and results from the FIRS, SK93, and MSAM-I, experiments are discussed. These experiments search for anisotropy in the cosmic microwave background over a range in angular scale from 180° to 0.5° and a range in frequency from 26 to 680 GHz. Emphasis is placed on the observing strategy and potential systematic errors. Contamination of the data by galactic sources is addressed. Future directions are indicated.

The results for all three experiments, as found by us and others, are given in the context of the standard CDM model, Q_{CDM}, ($\Omega_b = 0.05$, $H_0 = 50$ km/s/Mpc, $\Lambda = 0$, $n_s = 1$, $\Omega = 1$, no reionization) and the model-independent band-power estimates, δT_{l_e}. For FIRS, $Q_{CDM} = 19 \pm 5$ μK and $\delta T_{l_e} = 30 \pm 7$ μK with $l_e = 11^{+13}_{-9}$. For SK93 (statistical errors only), $Q_{CDM} = 14 \pm 4.3$ μK and $\delta T_{l_e} = 31 \pm 10$ μK with $l_e = 66^{+27}_{-20}$. For the *full* MSAM-I single-differenced data set, $Q_{CDM} = 20 \pm 4$ μK and $\delta T_{l_e} = 57 \pm 11$ μK with $l_e = 159^{+75}_{-76}$. For the *full* MSAM-I double-differenced data set, $Q_{CDM} = 18 \pm 4$ μK and $\delta T_{l_e} = 56 \pm 10$ μK with $l_e = 263^{+112}_{-82}$. The dependence of the results on data cuts is given.

1. Introduction

FIRS, SK93, and MSAM-I are designed to measure the anisotropy in the cosmic microwave background (CMB). These three very different experiments detect signals most economically described as produced by spatial variations in the CMB. In

[a] NASA/Goddard Space Flight Center, Code 685.0, Greenbelt, MD 20771
[b] Princeton University, Dept. of Physics, Princeton, NJ 08544
[c] University of Chicago, EFI, 5640 S. Ellis Ave., Chicago, IL 60637
[d] Global Science and Technology, Inc., NASA/GSFC, Code 685.0, Greenbelt, MD 20771
[e] Applied Research Corporation, NASA/GSFC, Code 685.3, Greenbelt, MD 20771

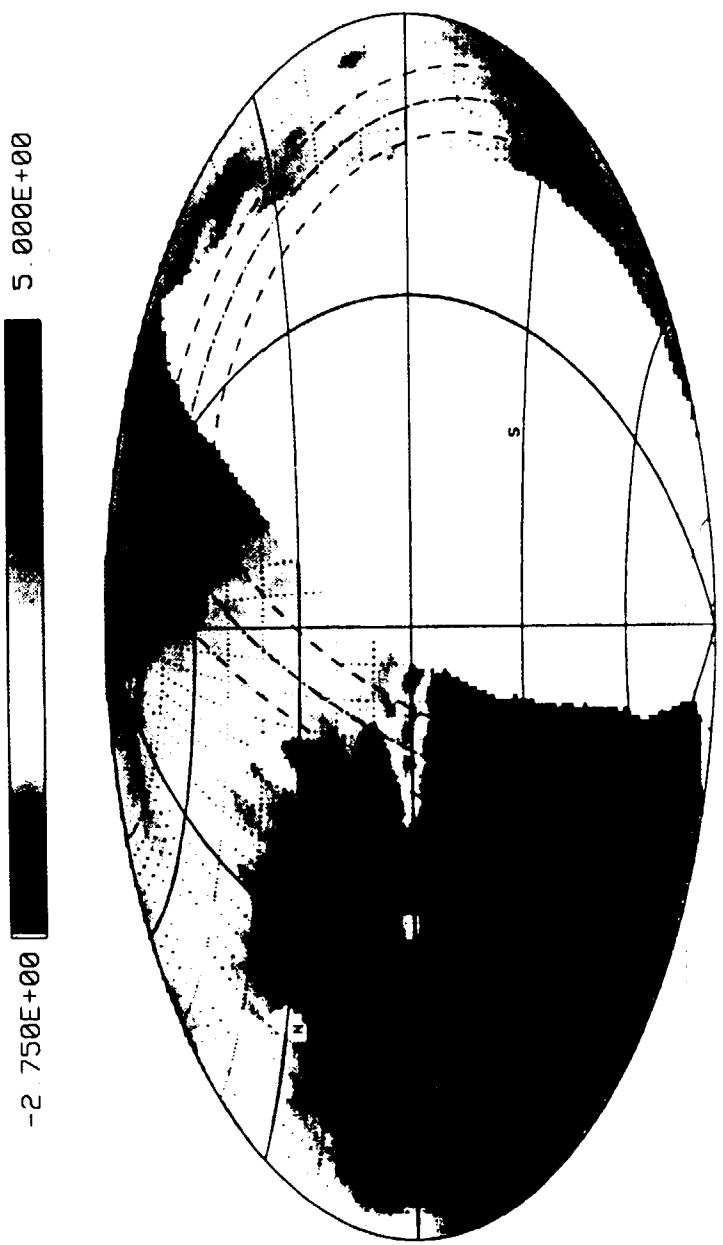

Figure 1. A map of the combined 1989 and 1990 FIRS coverage in Galactic coordinates. The dipole and Galaxy are clearly evident. The bright spot near $l = 190°$ and $b = 10°$ is Jupiter. This map is not yet ready for statistical analysis. The results described in this paper come from an analysis of the 1989 flight alone – a subset of this map.

the case of FIRS, there is a strong cross-correlation (Ganga et al.[1]) with the COBE DMR data (Bennett et al.[2] and Smoot et al.[3]) as well as an independent detection of anisotropy. To date, this is the only example of two completely independent experiments observing the same structure in the sky.

For SK93 and MSAM-I, the detections are convincing and the signals are more consistent with fluctuations in the CMB than anything else but it cannot be stated with "scientific certainty" that the anisotropy has a value of such and such. The case is fairly solid but not apodictic. This is primarily because the results have not been confirmed. As far as I am aware, at angular scales less than 4°[1], there are no published results of detections that have been confirmed either by a second separate observing campaign or by a completely independent group. Until there are confirmations, the data should be viewed with a healthy skepticism. Even after confirmation, one must be certain that the fluctuations have the correct frequency spectrum. Fortunately, the observing strategies for both SK93 and MSAM-I were designed to make confirmation relatively straightforward[2].

In this article, the quick overview of each experiment is given followed by some of the details that have not been emphasized elsewhere. The results from each experiment are given in a common language so that they may be compared to each other. The experiments are discussed in order of decreasing angular scale.

2. FIRS

2.1 Introduction

The Far Infrared Survey (FIRS) experiment began at MIT in 1982. The FIRS instrument is a balloon-borne four-channel bolometric radiometer. It has had three successful flights. The first, in October 1988, lasted only 8 minutes; however, useful data were obtained (Page et al.[6]). The second, in October 1989, has produced a map of the sky in the low frequency channel at 170 GHz. All of the results discussed in this article come from an analysis of this map. The data from the other channels are in various stages of analysis. Data from the third flight, in May 1990, are partially analyzed. The sky coverage for the combined 1989 and 1990 flights is shown in Figure 1.

The FIRS radiometer observes the sky at four frequencies (170, 290, 500, and 680 GHz) with a resolution set by the FWHM of the beam, 3.8°. The sky is viewed through a single aperture or horn; there is no beam switching. At a frequency of 4.5 Hz, the celestial flux is compared to the flux from a thermally stabilized internal reference. In one second, a difference in temperature of 450 μK can be measured with a signal to noise of one. To map a large region of sky, the optical axis spins about the zenith with a period of 40 s at an elevation angle of 45°. The motion of

[1] At large angular scales, TENERIFE[4] has been observing the same part of the sky for many years at 5.5°. The ability to detect CMB anisotropy at 15 GHz is encouraging given the projected level of galactic free-free emission.

[2] As of August 1994, I am aware of three intermediate angular scale experiments that have re-observed their sky coverage; SK93, MSAM, and PYTHON[5]. The results should be published soon.

the optical axis combined with the chopping action smears the beam to about 3.9°; an insignificant effect in all analyses. With a six hour flight, roughly 1/4 of the sky is mapped. The data are calibrated using the amplitude of the dipole measured by DMR. Descriptions of the experiment are given in Page[7] and Page et al.[8]

The biggest potential source of error with this observing scheme is that the offsets are large and they vary in time. The offset is the 'constant' part of the demodulated, or sky minus reference, signal. This is because a 'signal' is produced by everything skyward of the mechanism used to compare the sky to the reference. For instance, it is easy to see the optics cooling and the column depth of the atmosphere changing due to the bobbing of the balloon. In the 1989 flight, the offset was about 150 mK and varied about that much in one hour (it was re-zeroed every hour). The way around the offset problem for FIRS is to make the thermal time constants much longer than the rotation period.

Producing a map from the raw data is a time consuming process and, given the large offsets, care must be taken. The method we use was pioneered by Cottingham[9]. In essence, the slowly varying offset is found (and removed) by minimizing the total *variance* of the map, independent of the mean value of any given pixel. The fit is sensitive only to temporal signals, not spatial ones. In addition, one can compute the correlation introduced into the data by the fit. This has been done and we find that these correlations are small.

In the final map, there are 3500 1.3° × 1.3° pixels at galactic latitudes greater than 15°. The mean error bar is 260 μK. Thus, the offset is subtracted to about a part in 600. The subtraction is not perfect. If the map is examined on a pixel by pixel basis there is greater variation in the data than one expects from the error bars (which are derived from the distribution of the data). Bond has termed this 'white noise.' The origin of the noise is not known. We suspect it is not celestial but are not yet certain. All tests show that the excess variance is uncorrelated and close to white. Because of this, the map is not particularly useful for chi-squared type analyses unless the signals are very large. Fortunately, the signals from the CMB dipole and galactic dust are large.

If one assumes that the anisotropy is a random field, then spatial correlations within the map (auto-correlation) or between maps (cross-correlation) are the useful things to quantify. In our tests for systematic effects, we have not found any significant correlations produced by astrophysical foregrounds, the instrument (for instance, detector time-constants and cosmic ray hits or the chopper and the magnetic field), or the data analysis.

So far, the higher frequency channels in FIRS have been used only to rule out the possibility of galactic dust and atmospheric contamination of the 170 GHz data. In particular we find that the auto-correlation of dust near a 4° lag is about 100 $(\mu K)^2$ (in CMB temperature units) at 170 GHz for $|b| > 15°$. We also find that if one assumes the dust has the same temperature both on and off the galactic plane, then the spectral index is larger for dust off the plane (Ganga et al.[10]).[3]

[3] Dust emission may be characterised by $I(n, T_d) = \epsilon_0 \nu^n B(\nu, T_d)$ where T_d is the temperature of the dust, n is the spectral index, and $B(\nu, T_d)$ is the Planck function.

2.2 Cross-correlation with DMR

The cross-correlation between the DMR reduced galaxy ("fit technique") maps[2] and FIRS is described in Ganga et al.[1] The essence of the correlation is shown in Figure 2; the similarity of the cross-correlation between FIRS and DMR and the DMR auto-correlation is striking. With simulations we can show that the only way to get as significant a correlation is if both maps measure the same underlying sky. That is, the phases and amplitudes of the structure in the maps must be similar.

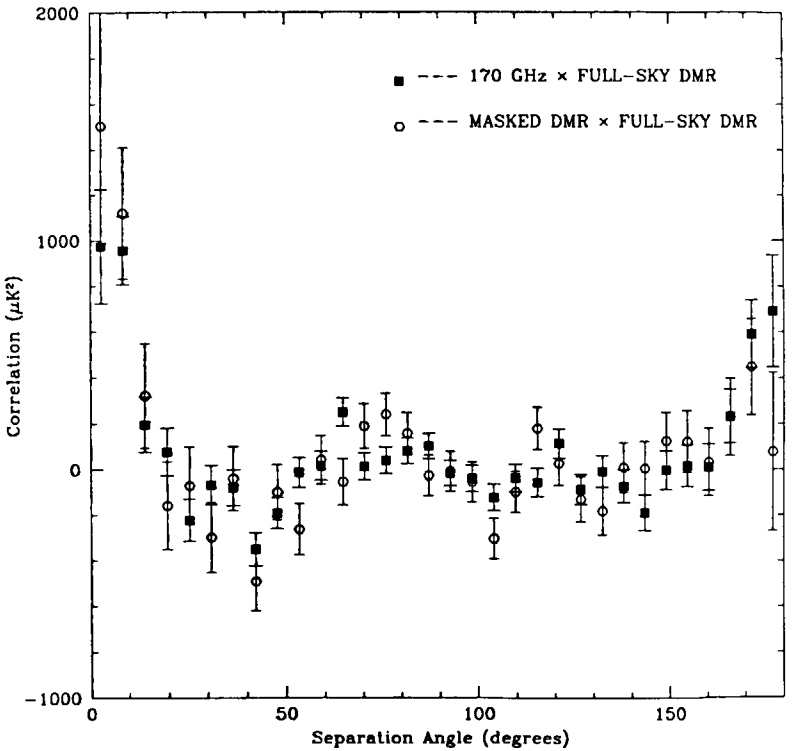

Figure 2. The cross correlation between the FIRS and DMR maps. The boxes are for the FIRS map correlated with the entire DMR map for galactic latitudes greater than 15°. The circles are for the masked DMR map (trimmed to have the FIRS coverage) correlated with the full DMR map. Note the similarity between the two correlation functions even though the two experiments are uncorrelated.

The important thing about the cross-correlation is that the potential systematic effects in the two experiments are very different; in some sense the experiments are uncorrelated. The primary galactic contaminant for FIRS (at 170 GHz) is interstellar dust emission and for DMR (at 53 GHz) it is galactic free-free emission. FIRS observes the sky with a single horn and compares celestial flux to a reference. DMR measures temperature differences all over the sky and then reconstructs a map. FIRS uses bolometric detectors, DMR uses a Dicke-switched heterodyne receiver. The FIRS data were taken in one night and the DMR data were taken over a year. There is no doubt that DMR is a far 'cleaner' result; there are fewer systematic problems and the DMR instrument is more stable than is FIRS's. But because of its finer angular resolution, comparable sensitivity (to 1 year DMR), and higher frequency, FIRS is an excellent check for DMR and provides complementary science.

2.3 Auto-correlation function

The FIRS data alone contain significant correlations. The auto-correlation function shown in Figure 3 is essentially the one shown at the meeting when the DMR results were announced. At that time, analyses by Bond were plagued by the 'white noise' and our two methods of analysis, described below, did not agree (this was traced to a bug in the code). Since then, a lot of work has been done; both methods now agree and analyses done by Bond[11] and us agree (with some minor exceptions discussed in the next section).

One may get a feel for the effect of the white noise by looking at the weighted *rms* of the map; it is ≈ 100 μK per 3.9° by 3.9° pixel. Given the DMR result, the expected *rms* is ≈ 50 μK. That is, the signal to noise per pixel is 0.5. By averaging over four pixels, the signal to noise is closer to one; in total, there are 380 such pixels.

Our analyses test models with a scale invariant spectrum, $P(k) \propto k^{n_s}$, $n_s = 1$, with the angular power spectrum given by (Bond and Efstathiou[12]),

$$C_l = Q^2 \frac{4\pi}{5} \frac{\Gamma\Big((2l + n_s - 1)/2\Big)\Gamma\Big((9 - n_s)/2\Big)}{\Gamma\Big((2l + 5 - n_s)/2\Big)\Gamma\Big((3 + n_s)/2\Big)}, \qquad (1)$$

where $Q = \sqrt{5C_2/4\pi}$ is a parameter that sets the scale, l is the multipole moment, and n_s is the index of the fluctuations[4]

In the first method, 20000 simulations of the sky with the same statistical weight and coverage as for the experiment are made. Next, the correlation function for each is found. Then, all the correlation functions are averaged together. Finally, the average correlation function is fit to the one made with the true data to find the best scale. The result is $Q_{CDM} \approx Q = 19^{+5}_{-6}$ μK. This method gives an estimate of the value of the best-fit correlation but it is not formally correct because it ignores

[4] The Q in Eq. (1) is called Q_{rms-PS} in Smoot et al.[3]. For experiments that probe angles as small as 4°, n_s should be set to 1.2 to get the C_l for CDM (the spectrum is still scale invariant, just treat n_s in Eq. (1) as a parameter). For all intents and purposes, we may think of Q as Q_{CDM} for FIRS.

correlation between bins of the correlation function and ignores the non-Gaussanity of the distribution in each bin (Cayon et al.[13]).

In the second method, both of these objections are overcome. We find the distribution of the Boughn-Cottingham statistic (Cottingham[9], Boughn et al.[14], Wright et al.[15]) given the model in Eq. (1) with $n_s = 1$ and the map. The result is $Q_{CDM} = 19^{+5}_{-5}$ μK. In an independent analysis based on Bayesian (as opposed to frequentist) methods, Bond[11,18] finds that $Q_{CDM} = 18.6 \pm 4.7$ μK.

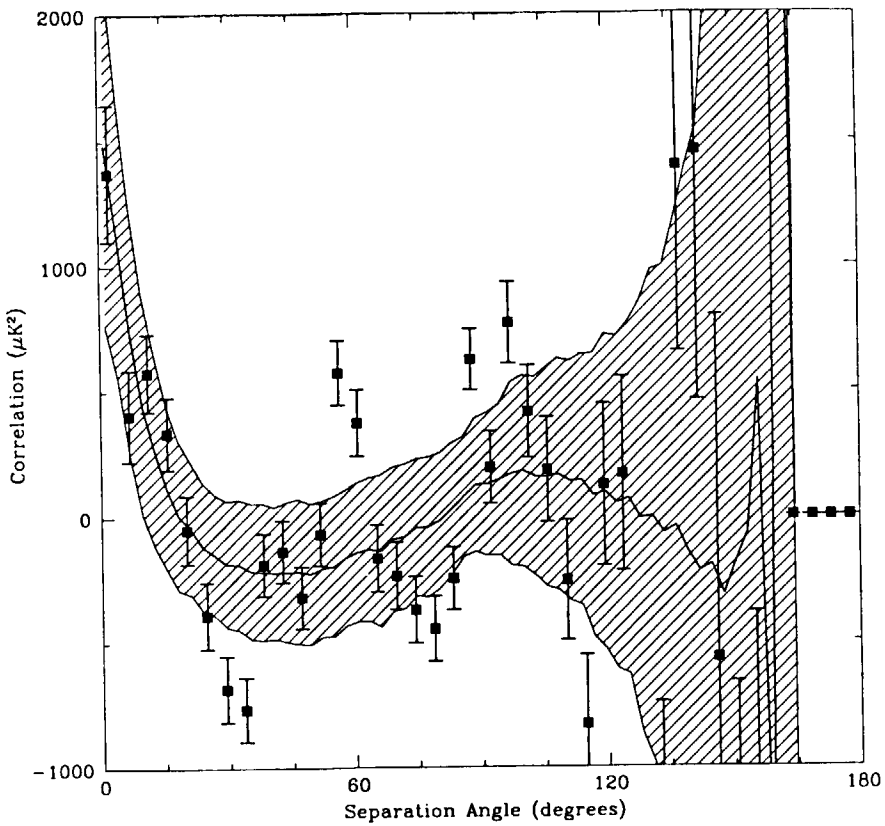

Figure 3. The FIRS auto-correlation function. The central continuous line is the best fit to the mean of 20,000 simulations of a scale invariant sky with $Q = 19$ μK in Eq. (1). The shaded swath is the 1σ deviation. The cutoff at 150° is due to the finite extent of the 1989 FIRS coverage.

The FIRS window function is $W_l = e^{-(l+.5)^2\sigma^2}$ where $\sigma = 0.028$. W_l extends from $l = 2$ to $l = 24$ where it falls to $e^{-0.5}$. Band-power estimates[18] give the value of the power spectrum in some band of multipole moments assuming a scale invariant spectrum for all l. In this article, we give the square root of Bond's estimates because the experimental error bars are linear in temperature, not temperature squared. A slight modification of Bond's formalism is given in Peebles[16]. We use the notation

$$\delta T_{l_e} = \frac{\delta T_{rms}}{\sqrt{I(W_l)}} = \frac{\sqrt{I(W_l C_l^*)}}{\sqrt{I(W_l)}} \tag{2}$$

where

$$I(f_l) \equiv \sum_l f_l \frac{(l+1/2)}{l(l+1)}, \quad l_e = \frac{I(lW_l)}{I(W_l)}, \quad \textit{and} \quad C_l^* = \frac{l(l+1)}{2\pi} C_l .$$

For an $n_s = 1$ model, Bond finds the band-power to be $\delta T_{l_e} = 29.7 \pm 7.1\ \mu$K at $l_e = 11$.

2.4 Spectral index and Q

It is possible to constrain the index, n_s, as well as the amplitude, Q, of the power spectrum given in Eq. (1) with the FIRS data. A method for doing this based on correlation functions is given in Ganga et al.[10,17]. It is particularly well suited to the FIRS data with its peculiar sky coverage, uneven weighting, and white noise. The correlation function, in effect, filters the data. For instance, if the bin at zero lag is deleted, as it is in all our analyses, then the white noise is essentially eliminated.

The results of the method are shown in Figure 4. The relative probability, or likelihood, of obtaining the FIRS auto-correlation function is given as a function of n_s and Q. While the limits on n_s are not particularly tight, it is pleasing that indices near 1.2 are favored. In addition, if one restricts oneself to $n_s = 1$, the results in section 2.3 are recovered. If white noise were contaminating the method, indices near $n_s = 3$ would be favored. In the future, this method will be extended to include the cross-correlation with DMR.

2.5 Comments and the Future

One of the most important lessons from FIRS is that despite the fact that the data are not particularly clean (they contain a noise component that is not understood), they contain cosmological information that can be quantified. It is only possible to get at this information because FIRS produces a map. All of the analyses focus on the spatial correlations within the FIRS map or between FIRS and DMR; the *rms* deviation within the map is ignored. Most analyses of experiments that do not produce maps use some form of the *rms* as the statistic. The correlation function of the measured ensemble of temperature differences – one of the signatures of a cosmic field – is not used. Another lesson from FIRS is that the comparison with DMR is only possible because FIRS produces a map.

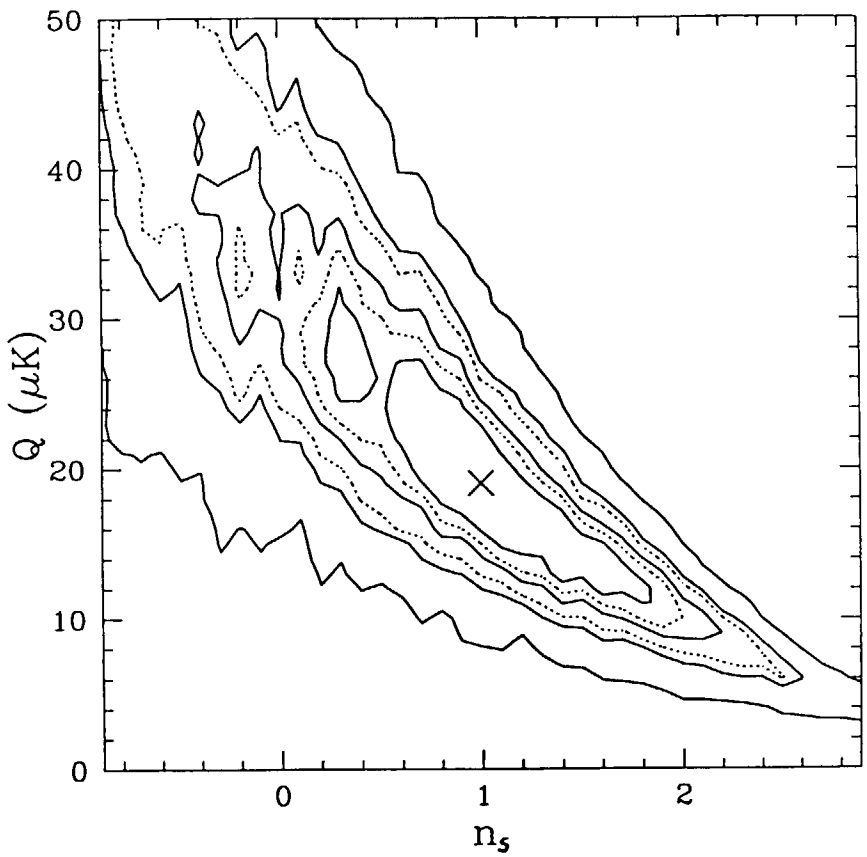

Figure 4. The likelihood of the FIRS data as a function of Q and n_s given in Eq. (1). The solid lines correspond to likelihoods of 0.05, 0.25, 0.5, and 0.75. The × at $(n_s, Q) \approx (1, 19\ \mu\text{K})$ is the maximum and the broken contours correspond to likelihoods of 0.34 and 0.68.

Although we know that there is correlated structure in FIRS (and, of course, DMR), the angular power spectrum is still not well constrained. For instance, the FIRS correlation is better explained by a Gaussian correlation function ($\theta_c = 13°$) than by Eq. (1). The data are simply not sensitive enough to distinguish between models. Even different analyses of the FIRS data do not give the same value for n_s. Bond[18] has done an analysis based on the power spectrum and found $n_s = 1.8^{+0.6}_{-0.8}$. While this is statistically consistent with our results, in principle he should find the exact same result. In addition, at some level, cosmic variance will not allow one to

distinguish between cosmological models using CMB data alone [19,20].

The current plan is to finish analyzing the existing data and then re-fly the experiment to produce maps of the whole sky. This program will take place at the University of Chicago.

3. SK93

3.1 Introduction

The Saskatoon experiment (SK93, aka BIGPLATE) uses a HEMT[5] based radiometer to observe the sky in three frequency bands (26-29, 29-32, 32-35 GHz) with a FWHM beam of 1.4°. Two polarizations are measured simultaneously for a total of six channels. A schematic is shown in Figure 5. The beam is formed by a cooled (15 K) corrugated horn and an ambient temperature off-axis parabola. The beam is steered on the sky with a computer-controlled large chopping plate that oscillates in azimuth at 4 Hz. The initial results from the experiment are reported in Wollack et al.[21] A full description of the instrument is given in Wollack (1994)[22].

This radiometer is very stable. The offset is small, on the order of 350 μK, and there is no discernible time variation over a period of two weeks. In principle, the experiment could be done by pointing the instrument at one position and letting the sky drift through. Before the observing campaign, the input to the radiometer was blanked-off and data were synchronously averaged with the chopper moving for 16 hours. No significant signal was found at any of the chopper harmonics (out to 12 times the fundamental frequency), indicating that there are no electronic offsets. If one computes the expected offset due to polarized emission from the chopper, then one gets nearly the measured result.

The radiometer is calibrated on Cassiopeia-A. The absolute flux of Cas-A is well known at frequencies below 31 GHz; it is a radio astronomy standard[23]. A power law with $S_\nu \propto \nu^{-0.77}$ gives an excellent fit to the 1 – 30 GHz data. We assume that this power law is still true up to 40 GHz. This is supported by a measurement at 31.4 GHz[24]. Measurements at higher frequencies[25,26] show some deviation, but the situation is not clear (this deviation would make our β more positive). Calibrating on celestial standard is convenient because the atmosphere, telescope efficiency, and temperature profile of the receiver (the gain is temperature dependent) are the same as when cosmological data are taken. We find that with the power law assumption, the calibration done in the lab agrees with the Cas-A calibration to better than 20%. The calibration from Cas-A [6] , including systematic effects, is accurate to better than 10%. The relative calibration between channels is accurate to 2%. These

[5] High Electron Mobility Transistor. We use the components developed my Marian Pospieszalski and collaborators at the National Radio Astronomy Observatory. The HEMTs simply amplify the incident radiation in much the same way an audio frequency transistor would. After amplification, the total power of the field is measured with a "square law" detector (actually a RF diode).

[6] There is a small HII region near Cas-A, 2311+611, that effects calibrations done in the evening at the 6% level.

errors are not included in the reported result. Cas-A is bright enough to allow us to make a beam map down to about 15 dB. The Cas-A beam map and the laboratory beam map agree to 0.02°, indicating that Cas-A is fully modulated. Finally, we can can check the absolute pointing using Cas-A; it is accurate to 0.1°.

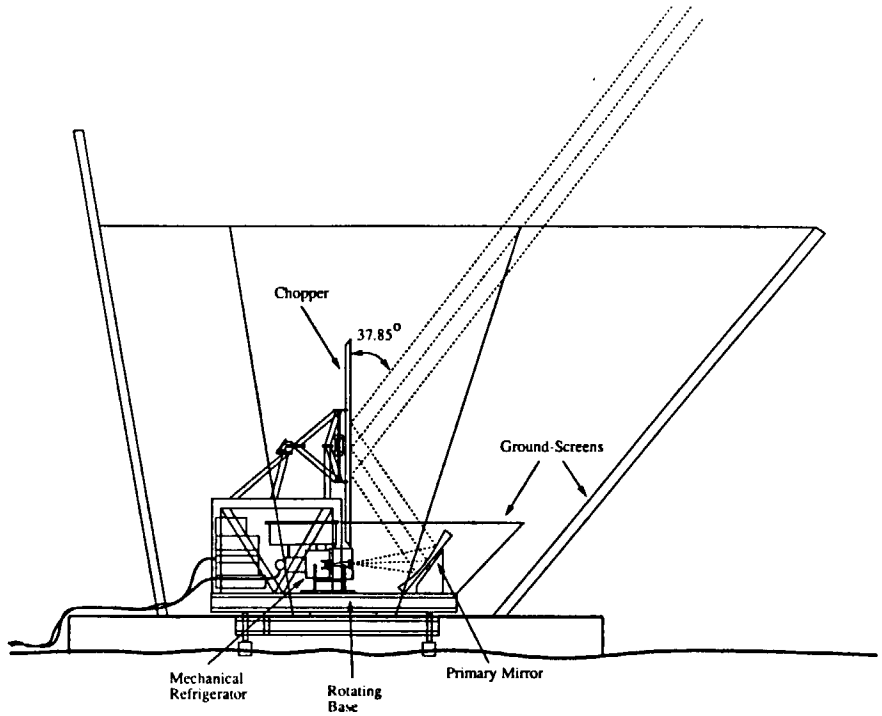

Figure 5. Schematic of the Saskatoon telescope with the 3 dB beam profile. The scale may be judged by the height of the 5 foot chopper. When wobbling, the inner ground screen and all the optics rotate. The latitude of Saskatoon, SK (52.14°) sets the zenith angle of the beam.

3.2 Scan strategy

In addition to the rapid scanning motion of the chopper, the optical axis is wobbled in azimuth about the north celestial pole. First it is pointed 4.9° east for 16 seconds and then 4.9° west for another 16 seconds, all the time at a constant elevation equal to the latitude of Saskatoon, SK.[7] As the Earth rotates, the celestial sphere drifts through the scanning beam. This east-west motion is maintained 24 hours a

[7] We also looked North on each scan. These data were not used.

day; data from the day and night are combined. The east-west wobble is designed to allow differentiation between diurnal signals which have a 24 hour period and those fixed to the celestial sphere which repeat at 12 and 24 hours. This allows us to determine if a signal is fixed to the Earth or the sky.

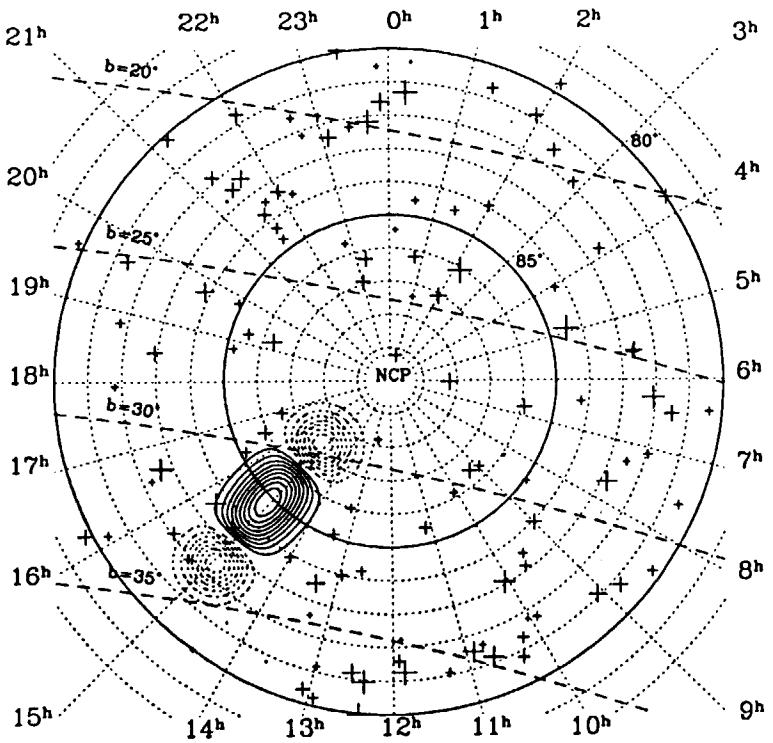

Figure 6. Beam pattern for SK93. Contours of the instantaneous beam profile are shown. Note how much it resembles a "double-difference" pattern (positive lobe:solid lines, negative lobes: dashed lines). The '+' signs mark the sources in Kühr et al. survey. The size of the symbol is proportional to the flux. Lines of constant galactic latitude are also shown.

The data stream is sampled synchronously with the chopper motion at sixteen times the chopping frequency. The demodulation is done in software by multiplying each sample by a number. We call the set of numbers a demodulation vector. By changing the vector, we can probe different spatial scales. We can also examine the quadrature signals which are useful indicators of systematic effects and atmospheric contamination. The chopped beam profile depends on the demodulation vector

and the phase of the sampling with respect to the motion of the chopper. The instantaneous (averaged over 0.25 sec) profile for a right ascension of 15^h is shown in Figure 6. Note how closely it resembles a "double-differenced" pattern. In the analysis, the data is averaged in 1^h bins. The full beam pattern for a bin is the instantaneous pattern averaged over 15° in right ascension. Note that there is relatively large overlap between bins near the pole. A single hot-spot near the north pole would show up in four bins. Because of the slight curvature in the pattern, data taken in the east are treated independently from those taken in the west.

It is convenient to use a normalization that allows for an easy interpretation of the data. For SK93, the beam is normalized so that the area under the positive lobe of the full chopped beam profile is one (this is very close to a normalization using the instantaneous profile). That is, a 1 μK change in a source filling the positive lobe gives a detected signal of 1 μK. In Wollack et al. the parameters of an effective window function for the "double differenced" beam are given. A plot of this approximation is shown in Figure 7. We have recomputed the window function by integrating over the full beam profile taking into account all known effects. Using the new window does not change any of our previous results.

3.3 Data analysis and interpretation

The most difficult aspect of the data analysis of ground experiments is establishing a robust and objective method for discarding data contaminated by the atmospheric emission. For SK93, this is done by examining the statistics of the "single-difference" data (or first harmonic). Physically, the first harmonic is a transverse temperature gradient. If the mean deviation of the gradient in a 17 minute period is larger than $\eta = 3$ mK, then the data are discarded. The details are given in Wollack[22]. The determination of the sky variance is fairly independent of η. In essence, one can eyeball the sky to surmise if the data will be good. If the sky is clear and cloudless and it is colder than −10 C, the data will be good. What is surprising is that there are some very cold days with a uniformly high overcast that also give good data.

To analyze the data, we model possible fluctuations with $\delta T_{rms} \propto \nu^\beta$. For the CMB, $\beta = 0$ and for free-free emission, $\beta = -2.1$. We consider only one fluctuating component. The best values for β and δT_{rms} are determined from the maximum of the likelihood. The error bars are given by the 16% to 84% range of the integral under the likelihood. Because of atmospheric variations and gain variations in the HEMT amplifiers on .1 sec time scales the data in the six radiometer channels are correlated. These correlations must be taken into account. The dominant effect of the correlations is to increase the error bar over what one would have otherwise reported (but see Dodelson & Kosowsky [27]).

With $\eta = 3$ mK, $\delta T_{rms} = 33^{+10}_{-9}$ μK and $\beta = -0.3^{+0.7}_{-1.2}$. With $\eta = 2$ mK, which includes 60% of the $\eta = 3$ mK data, we find $\delta T_{rms} = 40 \pm 11$ μK and $\beta = -0.3^{+0.7}_{-1.2}$. This is clearly consistent with the $\eta = 3$ mK data. $\delta T_{rms} = 33$ μK is the preferred number because more data that we believe to be sufficiently uncontaminated by the atmosphere go into determining it.

At 30 GHz, contributions to the variance from extra-galactic sources and from galactic free-free emission are not expected to be negligible. Most of the sources at 30 GHz will also show up in the Kühr et al.[28] survey at 5 GHz. In Wollack et al., we show that sources are expected to contribute 8 μK to δT_{rms}. Of course, there could be a whole population of unknown sources with inverted spectra that are not seen at 5 GHz. At this stage we cannot rule out such a class; we need more data at higher frequencies and smaller anglar scales. It is often pointed out that it is not prudent to rely on the Haslam[29] (0.41 GHz) and Reich & Reich[30] (1.4 GHz) maps to extrapolate possible synchrotron or free-free contributions to higher frequencies. Though these maps are extremely useful for crude analyses at 30 GHz, fluctuations in the spectral index may lead one to incorrect conclusions. In addition, the maps have their own set of systematic problems. When one convolves these maps with one's beam pattern, the details of the map's scan pattern and the base line drift become important. It is not at all clear how the results should be interpreted. The safest course of action is to rely on the frequency coverage within one's own experiment to determine the foregrounds. For SK93, there is not much frequency coverage, but it is sufficient to rule out free-free emission with 90% confidence. While this indicates that the fluctuations are from the CMB, clearly we need more data.

To find the band-power, the SK93 window function along with $\delta T_{rms} = 33^{+10}_{-9}$ μK is used in Eq. (1). The result is $\delta T_{l_e} = 31 \pm 10$ μK with $l_e = 66^{+27}_{-20}$. A convenient check of the analysis may be done using the band-power formulation for the *rms* amplitude of the Gaussian auto-correlation function. In the SK93 analysis, $\delta T_{GACF} = 41^{+16}_{-13}$ μK for $\theta_c = 1.2°$ or $l_c = 48$. Using[11]

$$\delta T_{l_e} = \delta T_{GACF} \frac{\sqrt{I(u^2 e^{-u^2/2} W_l)}}{\sqrt{I(W_l)}} \quad \textit{where} \quad u = \frac{(l+1/2)}{(l_c+1/2)}, \tag{3}$$

we find that $\delta T_{l_e} = 32$ μK. To find Q_{CDM}, we use Steinhardt's[30] angular power spectrum in Eq. (2). The result is $Q_{CDM} = 14 \pm 4.3$ μK.

3.4 Future and comments

It is clear that SK93 needs to be confirmed and that we need a broader frequency range to constrain the index of the fluctuations. In the winter of 1994, the same team used two radiometers covering the 25 to 45 GHz range to observe the same part of the sky. After a preliminary analysis, we report that essentially the same signal has been seen. The spectral index is consistent with the CMB and the error bar is reduced. The full results will be reported in Netterfield et al.[32] Future campaigns with still smaller beams are planned.

Using a generalization of the modulation scheme described above, we now measure over a broad band in l-space. In SK94, the beam throw to beam FWHM ratio is greater than eight and we use a triangular scan pattern instead of a sinusoidal one. Future analyses will be sensitive to the correlation function of the differences. It will be possible to constrain both the amplitude and slope of the power spectrum over a range of multipoles.

Since we are entering the era of precision measurements of the anisotropy, it is worthwhile to examine the experimental limitations at Saskatoon. The dominant statistical limitation is the sky coverage; we need more points. In the SK94 analysis, the statistical error bar is dominated by sample variance - just the fact that one is deducing the variance of the parent distribution (the CMB) from a finite number of samples[8]. The dominant systematic error that we cannot get around with better instrument design is the calibration. Using Cas-A, it will be difficult to do better than 6%.

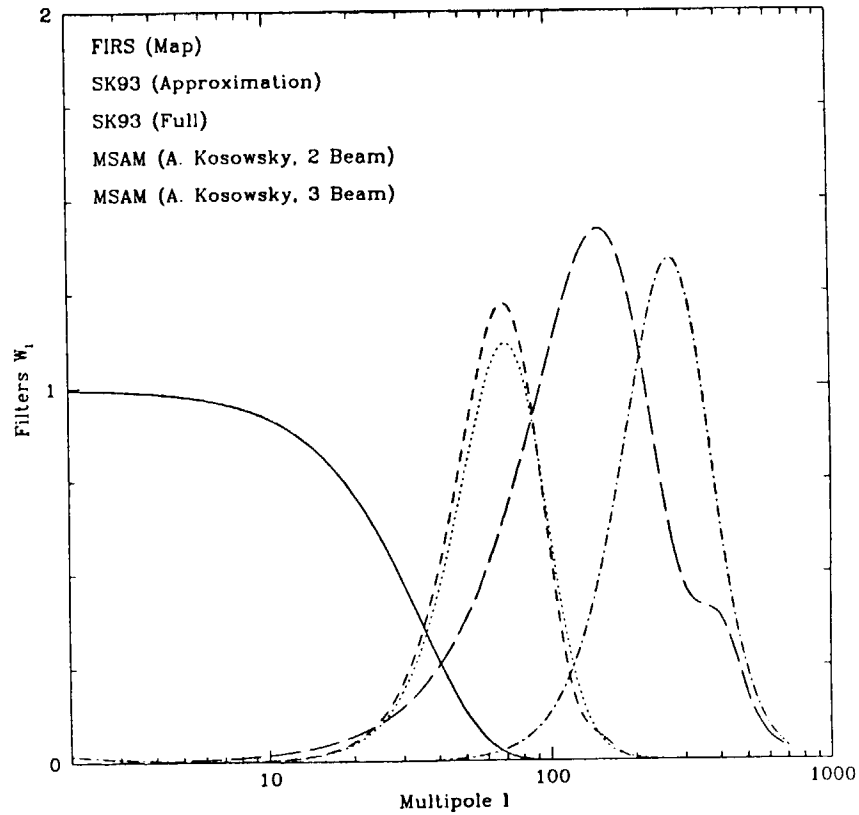

Figure 7. Window functions for FIRS, SK93, and MSAM-I. The smaller window that peaks near $l = 70$ is the approximation used in Wollack et al. The two MSAM-I windows were provided by Arthur Kosowsky. The one that peaks at smaller l is for the 2-beam demodulation pattern.

[8] The cosmic variance is the sample variance given full sky coverage.

4. MSAM-I

4.1 Introduction

The Medium Scale Anisotropy Measurement (MSAM) uses the FIRS detection system on a balloon-borne attitude-controlled off-axis Cassegrain telescope with a 0.5° beam. A schematic is shown in Figure 8. The frequency bands and beam size are fairly close to those used by the MAX[34] team. The collaboration is relatively young; there have been only two balloon flights. The first was in June 1992 and is described in Cheng et al[33]. The second, in June 1994, covering much the same area as the first, is still being analyzed. A number of papers on the instrument and various observations are in preparation.

The MSAM-I beam is switched, or chopped, on the sky by a rotating secondary mirror in a square wave pattern at 2 Hz. The total time per position is 0.125 sec and each transition lasts about 0.025 sec (included in the 0.125 sec). The mirror first points 0.69° to the left of the optical axis. Next, the beam moves back to optical axis, then it moves to the right and finally moves back to the optical axis. Because part of the beam forming is done by an over-moded elliptic concentrator, the beam is not particularly Gaussian. The measured profiles and data may be obtained via anonymous FTP from cobi.gsfc.nasa.gov[9]

With this optical arrangement, the beam moves over the primary when chopped. The beam in the left and right chopper positions overlap by roughly 80%, thus modest temperature or emissivity gradients will result in an offset (Fixsen et al. & Puchalla et al.[35]). Another source of offset is beam spill-over on the optical elements. In the first flight, the offset in the two low frequency channels (the ones primarily sensitive to the CMB) were on the order of 10 mK. The drifts in the offsets over the entire flight were less than 400 μK and were very nearly linear. By balloon standards, the offsets are very stable. In the data analysis, offsets were removed using Cottingham's method (see section 2.1).

The frequency channel placement in the MSAM-I radiometer was optimized for identifying astrophysical foregrounds given the detector sensitivity and the DIRBE and IRAS maps (the longest wavelength DIRBE map is at λ = 0.24 mm and the shortest wavelength MSAM-I channel is at λ = 0.44 mm. A large extrapolation is not required). To analyze the data, a ***physical model*** comprised of CMB fluctuations plus fluctuations in the emissivity of interstellar dust is used. The model fits the data fairly well; χ^2/ν = 237/292 for single-differenced data and χ^2/ν = 454/294 for the double-differenced data. As shown in Cheng et al., there is fairly good agreement between the IRAS prediction of dust and the dust component in the MSAM-I data. More importantly, there is little covariance between the CMB and dust models – the separation is clean. The CMB component of the fit is analyzed for anisotropy.

[9] Get the file /pub/data/msam-jun92/README. Be aware that the normalisation in the anonymous FTP archive is non-conventional but self-consistent. The 2-beam data plotted in Cheng et al. equals the data in the archive *multiplied by 2*.

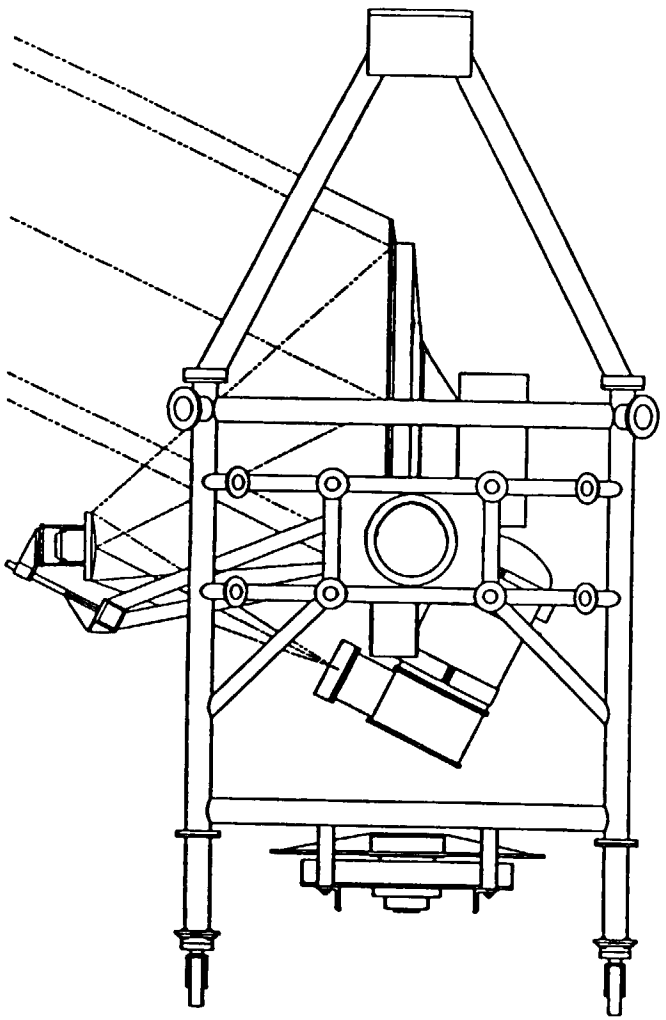

Figure 8. The MSAM-I gondola, without its ground screens. The chopper/secondary mirror is the optical element furthest to the left. Radiation from the sky is focused onto an cryogenic elliptic concentrator inside the dewar. To change the elevation, the chopper, mirror, and dewar rotate about the bearing which is shown schematically as two concentric circles in the middle of the figure. The momentum wheel is directly below the dewar.

Note that with the above switching scheme there are two statistically independent ways to demodulate the data. One can form the combinations left - right (single-difference) and center - (left+right)/2 (double-difference). Given the smooth scan described below, there are even more ways to demodulate the data stream. In principle, it is possible to form the correlation function of the data, especially for single difference data with its broad coverage in l-space.

4.2 Scan strategy

The primary goals of the scan strategy are to make the observations confirmable with minimal difficulty, to minimize the vibration of the radiometer, to produce a spatiotemporal filter that strongly rejects local sources of contamination, to keep the orientation between the optical axis and the earth as constant as possible, and to keep the optical depth through the atmosphere as constant as possible. An obvious, but sometimes overlooked, component to confirmation is accurate pointing information. Using a CCD camera and gyroscope, the position of the optical axis is known to an accuracy of 2.5 arcmin.

The details of the scan strategy have caused some confusion. There are three levels of modulation. On the fastest time scale (0.125 sec) the chopper moves the beam on the sky in the "double-difference" pattern described above. The center of the pattern is the principle optical axis of the telescope. The next level of modulation is the scanning, or wobbling, of the optical axis (entire telescope) in azimuth with an amplitude of 45′ and a period of 1 minute. In the final level of modulation, the center of the wobble tracks a point fixed to the celestial sphere for twenty minutes. The point is at a declination of 82°. It is tracked from 21′ east of the meridian to 21′ west of the meridian, through upper culmination. After tracking for twenty minutes, another point is picked up in the east. Figure 9 shows a plot of the coverage for the two beam demodulation scheme.

4.3 Sources

In the data in Cheng et al, there are some obvious "features" that have been called "sources." The features look the same as the point spread function of the beam. Initially these were thought to be members of a class of extra-galactic radio/sub-millimeter sources. A great deal of work has been done to identify possible candidates (particularly by Casey Inman and Matt Kowitt on the MSAM team) in existing catalogues of radio and infrared sources. So far, no viable candidate has been found.

A number of teams have observed the features with a variety of telescopes. Sarah Church and collaborators have looked with SuZie, Charles Lawrence and collaborators have looked with the OVRO 5.5m telescope, Tom Herbig and Dave Wilkinson looked with the Kitt Peak 12 meter, the SK93 experiment observes the same region of sky, and Lawrence Chernin and Douglas Scott have looked with the BIMA telescopes. These observations have been done over a wide range of frequencies and angular scales. Though there are no published results,[10] none of

[10] Church and Chernin & Scott are in the final stages of submitting their findings for publication.

the above experiments reports detecting a source; the jury is still out. A qualitative assessment of the reports is that the source cannot have a free-free spectrum that extents down to 30 GHz. None of the above experiments can tell if the feature is a compact bump in the CMB.

On another front, a couple of groups have simulated the MSAM-I observations. Matt Kowitt and Dave Cottingham assumed a Gaussian shaped power spectrum and predicted a very small probability of such features. Using a CDM model, which has relatively more power at small scales, Neil Turok and Paul Graham find that features suggestive of those seen in MSAM-I are not uncommon in their simulations (this, from non-Gaussianists!). Scott Dodelson finds the same thing.

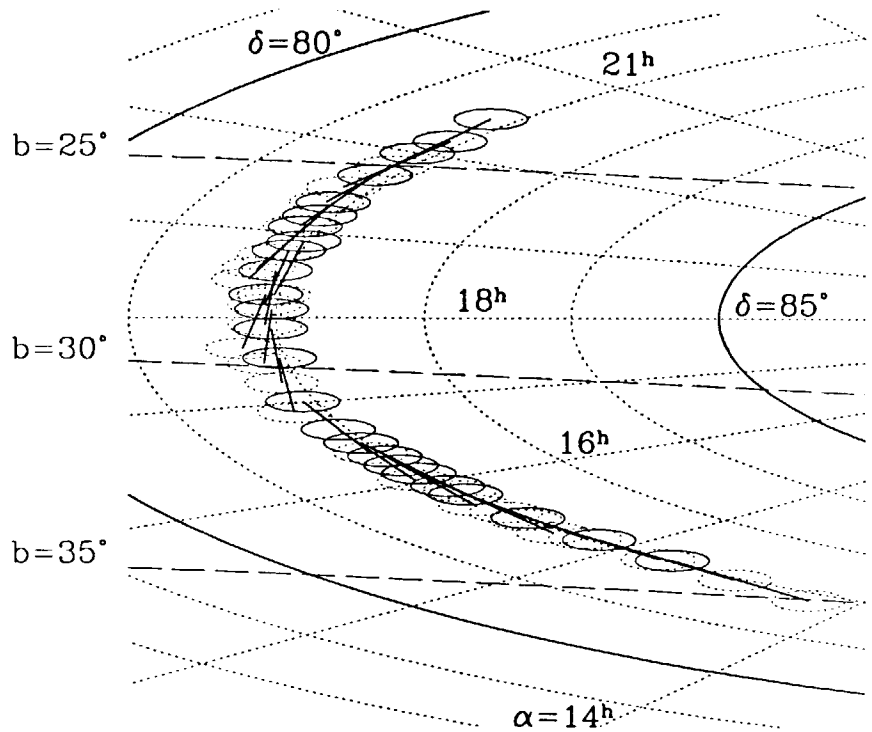

Figure 9. The MSAM-I sky coverage for the single-difference demodulation. One end of a difference pair is shown as a dotted line circle; the other as a solid line circle. The struts identify beam pairs. The data are analyzed using a binning six times as fine as the one shown here. Lines of constant galactic declination are shown for reference.

Given these three bits of circumstantial evidence, it is not unreasonable to entertain the possibility that MSAM-I observes CMB fluctuations in a CDM-like sky.

We wish to emphasize though, that the only way to resolve this question is with repeated observations over a wide range in frequency. One must also keep in mind the possibility that the sources may be experimental artifacts and that CDM is but one of many possible models.

4.4 Window function and results

Most of the window functions in print use the Gaussian beam approximation. While this is adequate for most analyses, it is not accurate. Arthur Kosowsky[36] has take the raw beam maps from the archive file, integrated them, and found the window functions. His results for the single and double -difference patterns are shown in Figure 7.

The results for the Gaussian auto-correlation function in Cheng et al. are $\delta T_{GACF} = 85 \pm 16$ μK at $\theta_c = 0.5°, l_c = 115$ and $\delta T_{GACF} = 74 \pm 12$ μK at $\theta_c = 0.3°, l_c = 191$. These error bars include a 10% calibration uncertainty. Using Eq. (3), these may be turned into band-powers. We find that $\delta T_{l_e} = 57 \pm 11$ μK with $l_e = 159^{+75}_{-76}$ for the single-difference data, and $\delta T_{l_e} = 56 \pm 10$ μK with $l_e = 263^{+112}_{-82}$ for the double-difference data. The band-powers may be converted into Q_{CDM} using Eq. (2). The results are $Q_{CDM} = 20 \pm 4$ μK for the single-difference data and $Q_{CDM} = 18 \pm 4$ μK for the double-difference data.

If the features are excluded, then the numbers for the single-differenced data are $\delta T_{GACF} = 39 \pm 11$ μK, $\delta T_{l_e} = 27 \pm 8$ μK, and $Q_{CDM} = 9 \pm 3$ μK. For the double-differenced data, the numbers are $\delta T_{GACF} = 58 \pm 14$ μK, $\delta T_{l_e} = 44 \pm 11$ μK, and $Q_{CDM} = 14 \pm 4$ μK.

4.5 Future

The MSAM-I experiment constitutes one part of the TopHat collaboration. For the second flight, John Ruhl and Jeff Jewell joined the team. The flight was successful and has substantial overlap with MSAM-I. Unfortunately, the dominant "feature" was not re-observed. Also, Peter Timbie's group at Brown (Khurram Farooqui, Grant Wilson, and Junwei Zhou) is building a novel low-frequency cryogenic radiometer (70, 90, 100, 140, & 160 GHz) that will use the same telescope, have the same beam, and observe the sky in the same manner. When this series of experiments is complete, $\delta = 82°$ will be thoroughly observed with a 0.5° beam from 70 to 680 GHz.

The TopHat team also plans a long duration balloon flight to make observations from a telescope mounted on top of the balloon. In addition to the above, this is being done with the Danish Space Research Institute and Bartol Research Foundation.

5. Directions

The goal of CMB anisotropy experiments for angles larger than about 0.2° should be to make a true map of the CMB with its associated power spectrum limited by cosmic variance. A true map is one that has had nothing but a DC level removed, similar to those made by DMR and FIRS. Detectors that are capable of achieving

this in reasonable amounts of time (1 year) are in hand, and all indication are that the detectors will improve. Robust strategies for producing maps are less well known. Many observers are beginning to investigate a range of methods. The advantages of a map are threefold. With maps, 1) experiments by different groups may be easily compared, 2) the statistics and power spectrum of the anisotropy are more easily determined, all angular scales are contained in a single measurement, and 3) foregrounds (both point-like and diffuse) are easier to recognize through, for instance, their statistics and their dependence on l, b, elongation etc.

So far, all the maps at frequencies near 90 GHz have been made from satellites or balloons. There are many proposed and active investigations along these well-trodden paths. It is not at all clear that one can produce a 90 GHz map from the ground but interferometers and very dry sites (eg. Antarctica) offer some promise. For this to work, the atmosphere, which at a good site is near 10 K, must be extraordinarily well-behaved to reliably map structure at 10μK over any appreciable angular scale. However they are made, maps limited by cosmic variance over a reasonable frequency span are a milestone for intermediate scale anisotropy measurements. Pushing the error bar per pixel below what is required to reach the cosmic variance limit will be useful, and perhaps necessary, for experiments investigating the polarization of the CMB. And who knows, maybe we'll find out that the CMB is not a Gaussian random field after all!

Acknowledgements

The three experiments described above have been in progress for over a decade in four institutions. We apologize, but there is not enough space to adequately thank the large number of people who have provide guidance and advice. Over the years, this work has been supported under NASA grants NAGW-1482, NAGW-2801, NAGW-1841, NAG5-2412, NGR 22-009-526, RTOP 188-44, NGT 50908, and NGT 50720 and a NSF grant PH 89-21378, and a NSF NYI grant to L. Page.

References

1. Ganga, K. M, et al. *ApJ.* **410** (1993) L57.
2. Bennett, C. L., et al., *ApJ.* **396** (1992) L7.
3. Smoot, G. F., et al., *ApJ.* **396** (1992) L1.
4. Hancock, S. et al., *Nature* **367** (1994) 333.
5. Dragovan, M., et al. *ApJ.* **427** (1994) L67.
6. Page, L. A., Cheng, E. S. & Meyer, *ApJ.* **355** (1990) L1.
7. Page, L. A., *A Measurement of the Cosmic Microwave Background Radiation Anisotropy*, (Ph. D. Thesis, MIT, 1989).
8. Page, L. A., et al., *Appl. Optics.* **33** (1994) 11.
9. Cottingham, D. A., *A Sky Temperature Survey at 19.2 GHz Using a Balloon Borne Dicke Radiometer for Anisotropy Tests of the Cosmic Microwave*

Background, (Ph. D. Thesis, Princeton University, 1987).
10. Ganga, K. M., *Exploring the Large Scale Anisotropy in the Cosmic Microwave Background Radiation at 170 GHz*, (Ph. D. Thesis, Princeton University, 1994). A paper on galactic emission is in preparation.
11. Bond, J. R. in *Cosmic Structure Formation & The Background Radiation*, Proceedings of the IUCAA Dedication Ceremonies, Pune, India, ed. T. Padmanabhan, (Wiley, 1992). And in *Evolution of Galaxies and Their Environments*, (Kluwer, 1992) 3rd Teton Summer School, ed. M. Shull, H. Thronson.
12. Bond, J. R., Efstathiou, G. *Mon. Not. R. Astr. Soc.* **226** (1987) 655.
13. Cayon, L., Martinez-Gonzalez, E. & Sanz, J. L., *Mon. Not. R. Astr. Soc.* **253** (1991) 599.
14. Boughn, S. P., et al. *ApJ.* **391** (1992) L49
15. Wright, E. L., et al. *ApJ.* **420** (1994) 1.
16. Peebles, P. J. E. *Proceedings from the Lake Louise Winter Institute*, (1994).
17. Ganga, K. M., et al. *Accepted for publication in ApJ.* (1994).
18. Bond, J. R. in *Relativistic Cosmology*, ed. M. Sasaki, (Academic Press, 1994); Proc. 8th Nishinomiya-Yukawa Memorial Symposium, Japan, October 1993.
19. Bond, J. R., et al. *Phys Rev Lett* **72** (1994) 13.
20. White, M., et al. *ApJ.* **418** (1993) 535.
21. Wollock, E. J., et al. *ApJ.* **419** (1993) L49.
22. Wollack, E. J., *A Measurement of the Degree Scale Cosmic Background Radiation Anisotropy at 27.5, 30.5 and 33.5 GHz*, (Ph. D. Thesis, Princeton University, 1994).
23. Baars, J. W. M. et al., *A&A* **61** (1977) 99.
24. Hobbs, R. W., Corbett, H. H., Santini, N. J. *ApJ.* **152** (1968) 43.
25. Kenney, J. D. and Dent, W. A., *ApJ.* **298** (1985) 644.
26. Mezger, P. G. et al., *A&A.*, **167** (1986) 145.
27. Dodelson, S. and Kosowsky, A, *FERMILAB-Pub-94/038-A, preprint*, (1994).
28. Kühr H., et al. *AJ.* **86** (1981) 854.
29. Haslam, C. G. T. et al., *A& AS.* **47** (1982) 1.
30. Reich, P. and Reich, W., *A& AS.* **63** (1986) 205.
31. The angular power spectrum for standard CDM, and a number of helpful suggestions, were kindly supplied by Paul Steinhardt of the University of Pennsylvania. The C_l are plotted in reference 19.
32. Netterfield C. B., et al. A paper on the confirmation of the SK93 results, *in preparation* (1994)
33. Cheng E. S., et al., *ApJ.* **422** (1994) L37.
34. Devlin M., et al., *ApJ.* **430** (1994) L1.
35. Fixsen D., et al. A paper on the MSAM-I instrument, *in preparation*, and Puchalla J., et al., a comprehensive paper on the analysis of MSAM-I data, *in preparation* (1994).
36. The MSAM window functions were kindly supplied by Arthur Kosowsky. A. Kosowsky was a graduate student at the University of Chicago; he is now at Harvard University.